Large eddy simulation of thermal effect on flow field around a building model with a scale ratio of 1:1:2

Yi Zhao[1], *Ruibin* Li[1], *Xusong* Hu[1], *Naiping* Gao[1*]

[1] School of Mechanical Engineering, Tongji University, Shanghai, China

Abstract. Urban overheating caused by urban heat island (UHI) effect has a negative impact on energy consumption, human health and urban air quality. This interaction between the approaching and the buoyancy-driven flows significantly alters the flow patterns around the building, consequently impacting the ventilation and dispersion of pollutants in urban areas. This paper utilized large eddy simulations to investigate the effects of buoyancy flow on the flow field around an isolated cubic building with heated surfaces. Wind tunnel experiments were also conducted to validate the simulation results. Under low wind speed conditions, the study utilized Richardson numbers (*Ri*) to quantify the relative contribution of forced convection and buoyancy flow. The *Ri* ranged from 0 to 4.00, indicating a transition in the flow field from being predominantly influenced by forced convection to being predominantly influenced by mixed convection. The windward, leeward, and all walls of the building were heated individually and compared with an isothermal building. The velocity, temperature and turbulent kinetic energy field were analysed. Significant changes in the flow field characteristics were observed under low Reynolds numbers and high surface temperatures. The thermal effects on the flow patterns led to variations in the length of the reattachment and recirculation zone.

1 Introduction

With the drive of industrialization and economic development, urbanization continues to progress worldwide. As urbanization accelerates, cities face a common challenge known as the urban heat island (UHI) effect. It is expected that extreme hot and humid weather conditions will increase in the future, leading to even hotter and more oppressive cities compared to surrounding areas, thereby exacerbating the UHI effect [1]. Moreover, UHI effects contribute to increased energy consumption and heighten the risks associated with heat-related deaths. Solar radiation is a major factor contributing to UHI. In rural areas, there is a high vegetation coverage, where plants absorb solar radiation energy and release moisture through transpiration, leading to a decrease in surface temperature. However, in urban areas, factors such as buildings, human activities, and industrial emissions disrupt the absorption and release processes of solar radiation. Urban surfaces typically possess higher thermal conductivity and capacity, enabling them to absorb and store solar energy. Furthermore, high-rise buildings in cities impede airflows, leading to heat accumulation. Daytime temperatures and humidity are higher than those at nighttime, making the daytime crucial for studying urban thermal dynamics. During the daytime, the surfaces of the building are exposed to solar radiation, causing surface temperatures to rise, and the thermal effect simultaneously alters wind speed and airflow patterns. The ventilation and dispersion of pollutants in urban areas are significantly impacted by the structure of the flow field. Factors such as airflow velocity, direction, and distribution play a vital role in the design of urban ventilation systems. Additionally, vortices and turbulence in the flow field structure can have an impact on the dispersion and mixing of pollutants.

In comparison to other building configurations, the isolated building has a simpler structure but exhibits significant airflow characteristics in its surroundings. Reynolds-Averaged Navier-Stokes (RANS) and Large Eddy Simulation (LES) are the most commonly used turbulence models in building aerodynamics. While RANS models are widely employed in various applications, LES is better suited for simulating complex flow phenomena around buildings, as it has the capability to capture transient features of the flow field. Murakami et al. [2] were the first to apply LES to predict the flow field around a cubic building in the atmospheric boundary layer. Okaze et al. [3] obtained high-quality measurements of fluctuating velocity and mean velocity around an isolated building at a scale of 1:1:2 using wind tunnel tests and LES.

Since *Re*-independence hypothesis was put forward, many investigations tried to find the corresponding critical *Re* for different situations when using the wind tunnel test to study the airflow patterns in urban areas. Lin et al. [4] discussed the critical *Re* values to achieve the *Re*-independent in street canyons with different aspect ratios. They found critical *Re* value for deep street canyon increased with aspect ratio. Tsalicoglou et al. [5]

* Corresponding author: gaonaiping@tongji.edu.cn

obtained the critical *Re* of 7090 for the step street canyon by wind tunnel tests. Allegrini et al. [6] measured the critical *Re* of 13000 for the flat canyon.

However, based on the literature review conducted so far, most wind tunnel tests and numerical simulations have focused on the flow patterns around the isolated building under isothermal conditions. Due to the numerous challenges associated with reproducing solar radiation in wind tunnels and water tunnels, only a limited amount of study has been dedicated to examining the flow characteristics around the isolated building under the influence of thermal effects through wind tunnel tests and within urban street canyons. A comprehensive investigation of flow characteristics around the isolated building under non-isothermal conditions is currently lacking. Therefore, a thorough analysis of wind tunnel test data and validated numerical simulation results of wind thermal fields around buildings with thermal effects is a meaningful endeavour.

The aim of this study is to comprehensively investigate the flow field around an isolated building, considering both forced-convective and buoyancy-driven flows. Using a combination of LES and wind tunnel tests, we reveal the flow field, airflow paths, vertical momentum flux, and turbulence kinetic energy distribution under varying heating conditions. We use a 1:1:2 cuboid; during wind tunnel tests, a heating film is applied to elevate the surface temperature of the building. Subsequently, the windward wall, leeward wall, and all building walls are heated ranging from 20 °C to 95 °C at varying incoming flow velocities, allowing for comparisons with the flow field around an isothermal building. The Richardson number (*Ri*) is employed to assess the dominance of natural convection and forced convection around the building, ranging from 0 to 4 in our study. Furthermore, we track the variation in the scale of the vortex region and the trajectory of the vortex centre across investigated cases, ensuring detailed flow field characterization.

2 Outline of CFD simulation

2.1 Governing equations

The numerical simulations in this study were performed using the CFD software Ansys Fluent that has been adopted in recent studies. In LES, the computation resolves the large-scale fluctuations, while the influence of small-scale fluctuations on the large scales is modeled. LES employs filtering methods to separate the small-scale fluctuations in turbulence, and its governing equations involve the application of filtering operations to the instantaneous motion of the Navier-Stokes equations.

2.2 Computational domain and grid

As shown in Fig. 1, a rectangular computational domain is established around the isolated building with dimensions of $31H_b(x)$ ×$21H_b(y)$ × $12H_b(z)$, where H_b represents the width of the isolated building. The dimensions of the isolated building model are 0.2 m (length) × 0.2 m (width) × 0.4 m (height), while the prototype dimensions are 10 m (length) × 10 m (width) × 20 m. This results in a scale ratio of 1:50. The computational domain dimensions follow the recommendations of COST. The origin of the coordinates is positioned at the leading edge of the isolated building on the ground, as indicated in Fig.1. The blockage ratio in the direction of the incoming flow is kept below the recommended 3% by the AIJ within the computational domain.

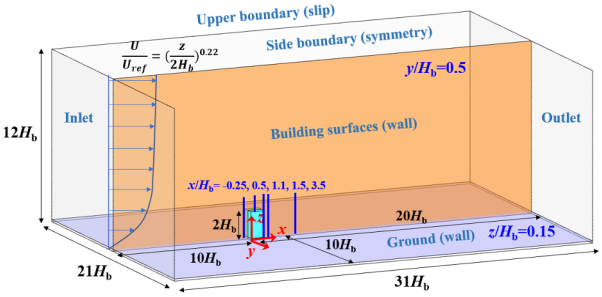

Fig. 1. Diagram of computational domain and the location of key lines and slices.

In this study, three distinct structured grids (coarse, medium, and fine) were generated using ANSYS ICEM CFD 19.0. Their respective cell numbers are approximately 3 million, 7 million, and 16 million. The Index of Quality (IQ) is employed to determine whether the mesh quality of the LES satisfies the solution requirements. IQ is defined as the ratio of resolved kinetic energy to the total kinetic energy. The mean values of IQ for all measurement lines are above 85%, surpassing the recommended threshold for LES. Considering both grid performance and computational costs, the medium grid is selected for the subsequent LES in this study.

2.3 Solver setting

The SIMPLE solver is utilized for pressure-velocity coupling. A second-order scheme is employed for pressure interpolation, while a bounded central differencing scheme is used for spatial discretization of the momentum equation. The transient formulation utilizes a bounded second-order implicit scheme. The Smagorinsky-Lilly model is utilized, and the value of the Smagorinsky constant (C_s) is determined based on previous LES studies on flow around buildings which suggested a value of C_s=0.12. Therefore, in this study, C_s=0.12 is adopted to investigate the flow field around the isolated building. And, the turbulent Schmidt number $\mu_t$was set to 0.5 [40]. The velocity fluctuations at the inlet boundary are computed using the Vortex method. The Courant numbers for all grids are maintained below 0.9, and the range of time steps Δt corresponding to different cases is 0.003 to 0.009.

2.4 Case description

The LES analysis examines the evolving patterns of the flow field surrounding an isolated building under the

combined effects of varying surface heating temperatures (45 °C, 75 °C, 95 °C, with a reference temperature T_{ref} set at 20 °C), distinct incoming flow velocities (0.5 m/s, 1 m/s, 2 m/s) at building height, and specific heating configurations (isothermal, windward wall heating, leeward wall heating, and all-wall heating). The incoming flow direction aligns perpendicularly to the windward wall of the isolated building. In general, *Re* of airflows in the wind tunnel is much lower than that of actual atmospheric flows. Thereby, *Re* of full-scale and model-scale cannot be equal. The assumption of *Re*-independence was first proposed by Townsend, that is, when the *Re* is large enough, the flows are also similar under the condition of geometric similarity.

The interplay between forced convection and natural convection is characterized by the Richardson number, *Ri* [24], which ranges from 0 to 4 in this study. The wall temperature and incoming flow velocities correspond to the Reynolds number (*Re*) and *Ri*. Smaller *Ri* values signify forced convection, whereas larger *Ri* values indicate mixed convection. For instance, "LEE-0.5-45" denotes heating of the leeward wall to 45 °C with an incoming flow velocity of 0.5 m/s at the H_{ref}. "ISO-0.5" indicates an absence of heating with an incoming flow velocity of 0.5 m/s at the H_{ref}. Likewise, "WIN" represents heating of the windward wall, while "ALL" signifies heating across all walls.

$$Ri = \frac{\beta g H_{ref}(T_w - T_{ref})}{U_{ref}^2} \quad (1)$$

$$Re = \frac{U_{ref} H_{ref}}{\upsilon} \quad (2)$$

3 LES validated by wind tunnel test results

The LES results were validated by comparing them with the measured values obtained from wind tunnel tests conducted at TJ-1 wind tunnel. The profiles were obtained along vertical lines by selecting the wind speed and temperature results at x/H_b = -1, 1.75, 2.5, and 3.5 from the wind tunnel tests. While this paper involves a variety of cases, the differences in the results between the two methods, i.e., numerical and experimental, are similar. Therefore, only the ISO-0.5 is selected to compare the normalized time-averaged velocity. On the windward side measurement line at x/H_b = -1, the experimental results for the normalized mean velocity were slightly higher than the simulated results. However, the remaining measurement lines demonstrate a high level of consistency between the two methods. Upstream of the building, the profiles are significantly affected by the inlet conditions, and the LES and experimental settings are not perfectly aligned.

4 Results

4.1 Non-heated walls

To provide a reference for the airflow patterns discussed in the subsequent sections, we will briefly examine the airflow patterns around an isothermal building. Fig. 1 presents the airflow patterns on the vertical central plane at $y/H_b = 0.5$ and the horizontal plane at $z/H_b = 1$. As the incoming wind approaches the windward wall of the building, the airflow disperses progressively upward, downward, and laterally. The stagnation point is observed at approximately 2/3 of the building height. Around the edges of the building, the airflow experiences significant horizontal and vertical acceleration. The separated flows reattach at the roof and leeward sides. Only the airflow above the stalled streamline can bypass the building, while a distinct curved shear layer forms on the roof surface [42]. Additionally, downward-moving airflow generates vortices near the ground surface.

For ease of explanation in the following sections, we refer to the vortex at the bottom corner of the windward side as the horseshoe vortex, the separation bubble at the top of the building as the top vortex, and the vortex on the leeward wall as the wake vortex. Three-dimensional streamlines. The top vortex sheds downstream at approximately the height of the building. The vortices generated within the shear layer fundamentally alter the flow field near the building and the recovery of the far wake. On the windward side, near the ground surface, the horseshoe vortex opposes the incoming flow direction, resulting in a low-speed region where the two opposing flows converge near the ground. The horseshoe vortex extends to both sides of the building, creating high-speed regions at the sidewall edges where lateral vortices form. A clockwise-rotating vortex exists within the recirculation region on the leeward facade of the building. it can be observed that the length of the recirculation region extends approximately 0.4 m behind the leeward wall of the building, and the flow outside the recirculation region returns to a normal pattern. However, within a range of approximately 1.3 m behind the leeward wall of the building, the airflow velocity remains lower than the incoming wind speed.

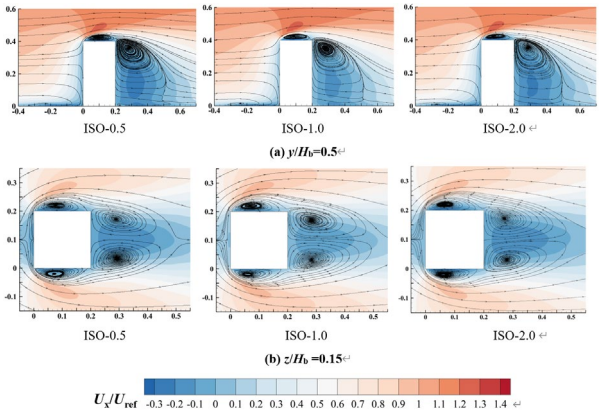

Fig. 1. Time-averaged airflow streamlines colored by the normalized time-averaged U_x over (a) the vertical central plane at y/H_b=0.5, and (b) the horizontal plane at z/H_b =0.15 (*Ri*=0) (the dimensions are in [m])

4.2 Leeward wall heating

Compared to isothermal conditions, heating the leeward wall induces a vertical upward motion, which affects the low-speed air within the recirculation region, as

depicted in Fig. 2. This air is drawn into the heated surface and enters the thermal plume, causing a change in the flow direction near the wake, primarily moving upward towards the leeward wall. Particularly, under the Ri=4.00 condition, the thermal plume near the leeward wall continuously rises, leading to a small cavity behind the roof edge with a counterclockwise-rotating corner vortex. Additionally, the top vortex shows an inclined upward trend.

Furthermore, turbulent kinetic energy (k) serves as an indicator of the magnitude of vertical motion ($<U'W'>/U_{ref}^2$). In most of the investigated cases, the location of the maximum absolute value of $<U'W'>/U_{ref}^2$ coincides with the location of k_{max}. Under the Ri=2.94 and 4.00 conditions, the magnitude of vertical velocity within the recirculation region increases significantly. As shown in Fig. 18, heating also results in a significant widening of the free shear layer's thickness due to diffusion, leading to a certain increase in k. The maximum turbulent kinetic energy (k_{max}) is observed at the trailing edge of the building roof and follows the vortex transport in a clockwise direction. However, the higher k at the center of the wake suggests that the disturbance caused by vortex shedding decays from the center to the downstream.

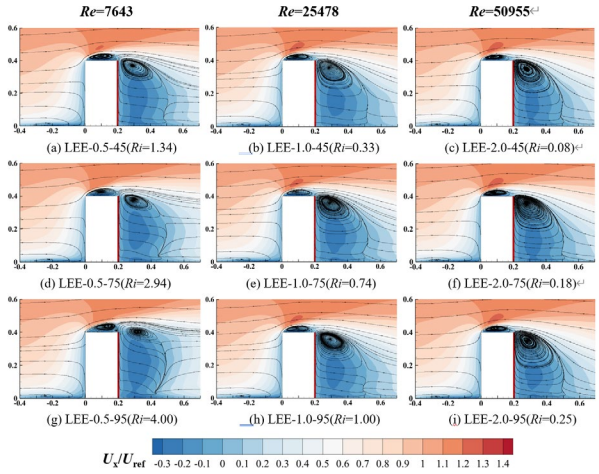

Fig. 2. Time-averaged airflow streamlines colored by the normalized time-averaged U_x over the vertical central plane at y/H_b=0.5 (the heated wall is represented by a red line; the dimensions are in [m]).

When the leeward side is heated, the interaction between the incoming flow at ambient temperature on the roof and the warmer air on the leeward side causes the warmer air to be washed downstream. This phenomenon highlights the influence of heating on the transport of heat downstream. Consequently, an elongated region with higher temperatures forms at the trailing edge of the roof. This elongated high-temperature region is clearly visible at the trailing edge of the roof under Ri=2.94 and 4.00 conditions (Fig. 3). However, this phenomenon is less distinct when Ri<0.33.

A link exists between heat and momentum transfer: areas with increased turbulence levels promote heat transfer. Concurrently, the temperatures near the leeward wall decrease rapidly. It is noteworthy that most of the heat is not carried into the wake through the recirculation region; instead, it is vertically carried away by the thermal plume.

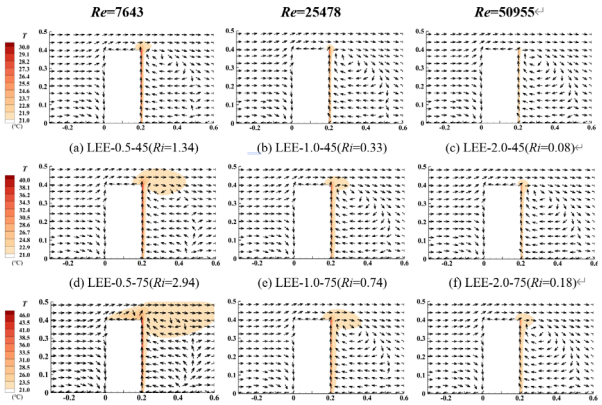

Fig. 3. Time-averaged velocity vectors and temperature over the vertical central plane at y/H_b=0.5 (the dimensions are in [m]).

4.3 Windward wall heating

In contrast to heating the leeward wall, the heating of the windward wall exhibits distinct characteristics. As depicted in Fig. 4, under conditions of low Re (Re=7643), the thermal plume displays two separate trajectories. A segment of the plume is directed towards the leeward side from the lateral direction, affected by the incoming airflow. Simultaneously, another segment of the plume enters the roof shear layer. In the cases of Ri=2.94 and 4.00, the thermal plume enters the wake region from the lateral side, and low-speed air is drawn into the thermal plume. It can be observed that the flow direction of near wake is upward towards the leeward wall (Fig. 4).

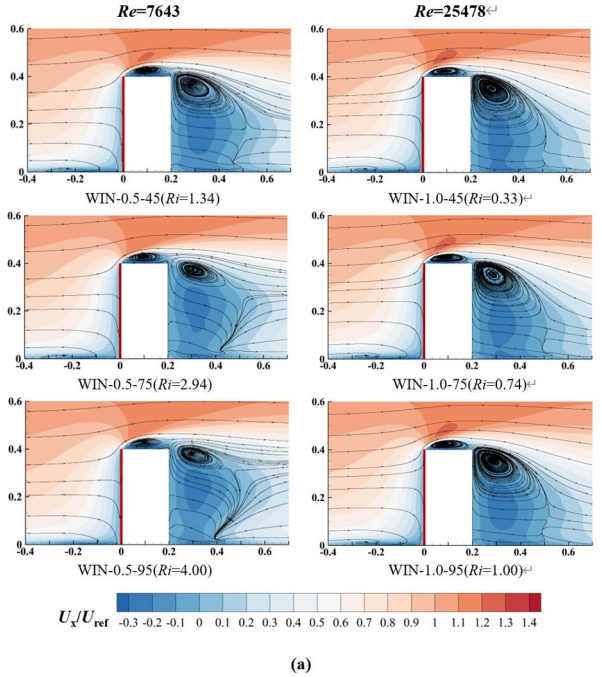

(a)

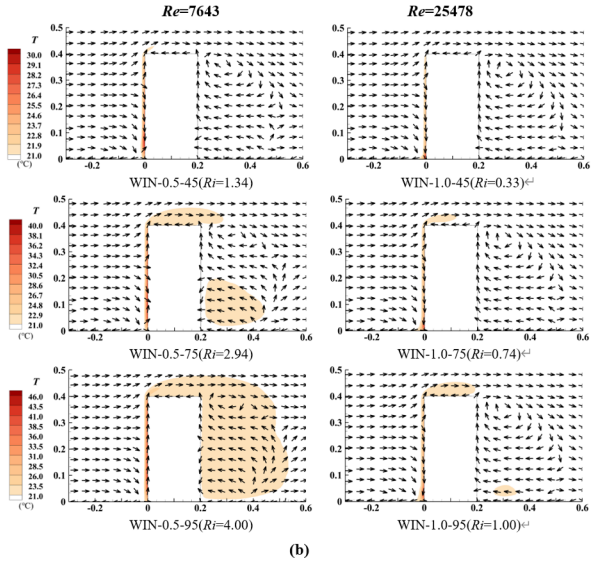

Fig. 4. (a)Time-averaged airflow streamlines colored by the normalized time-averaged U_x and (b) time-averaged velocity vectors and temperature over the vertical central plane at y/H_b=0.5 (the heated wall is represented by a red line; the dimensions are in [m]).

When the windward wall is heated, the low-speed incoming airflows at ambient temperature carry the high-temperature airflows from the windward side to the upper and leeward side of the building. Below the point of stagnation, the airflow moves along both sides towards the leeward side. Compared to the non-heated condition, in the cases with an incoming wind speed of 0.5m/s, as the wall heating temperature increases, the extent of the low wind-speed zone near the wake region of the isolated building gradually diminishes. As depicted in Fig. 5, at incoming wind speeds of 0.5 m/s and 1 m/s, an elevated temperature on the windward side leads to a gradual movement of heated airflow along both sides of the building towards the leeward side. Consequently, a subtle heating effect emerges within the airflow of the nearby wake region. Nevertheless, as the incoming wind speed increases to 2 m/s, even though the heating temperature on the windward wall is heightened and heated airflows towards both sides of the building, the impact of the heated airflow on the temperature of the airflow in the nearby wake region remains minimal. This limited effect can be attributed to the higher wind speed, which causes a rapid decrease in the temperature of the heated airflow, consequently constraining its effective reach.

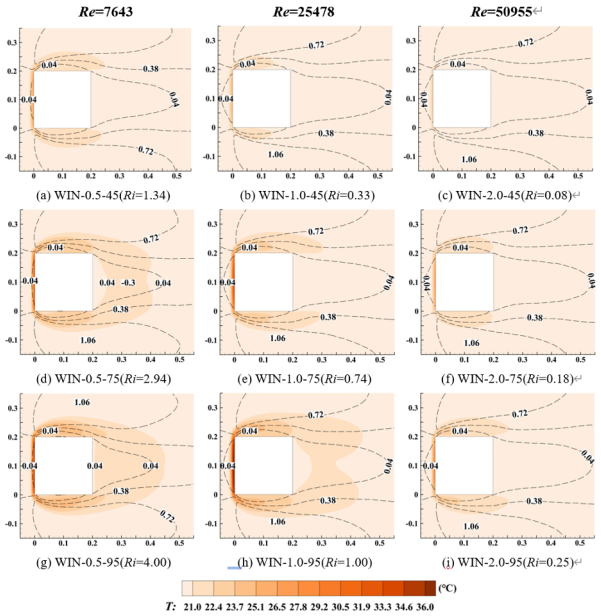

Fig. 5. Time-averaged temperature over the horizontal plane at z/H_b=0.15 (the long-dashed lines represent the contour of the normalized time-averaged U_x; the dimensions are in [m]).

4.4 All-walls heating

When all walls are heated (including side walls), the flow structures on the vertical plane undergo changes due to the increasing buoyancy. These changes are particularly notable at low *Re*. In the case of *Ri*=1.34, the wake vortex is disrupted by the buoyancy flow moving towards the windward wall, while the top vortex remains intact. Despite that, the deformation of the flow field caused by mixed convection has already occurred in the near wake, and the recovery of the flow field in the far wake requires the formation of new attached starting points, which are clearly visible in Fig. 6. For *Ri*=2.94 and 4.00, both the wake and top vortex structures are disrupted, and the vortex structures cease to exist. The stronger the vortices, the higher the inertial forces, necessitating a stronger buoyancy flow to dissipate the vortices.

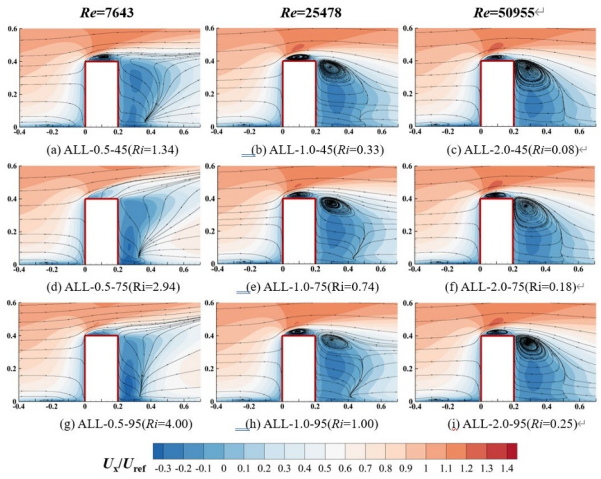

Fig. 6. Time-averaged airflow streamlines colored by the normalized time-averaged U_x over the vertical central plane at

y/H_b=0.5 (the heated wall is represented by a red line; the dimensions are in [m]).

In the conditions where all walls are heated, at *Ri*=0.08, the airflow temperature remains unchanged within the recirculation region. However, in the other conditions, there is a noticeable increase in temperature on the roof and leeward side of the building. Specifically, in the case of *Ri*=2.94, the temperature at the leading edge of the roof is elevated. This results from a combined effect of heating the roof and the incoming wind transporting the high-temperature airflow from the windward side to the top of the isolated building. Consequently, influenced by the thermal plume, the airflow over the roof undergoes a transformation, adopting an oblique upward motion. Simultaneously, within the recirculation zone, the temperature of the airflow increases due to the synergistic impact of the heated leeward wall and the warm airflow conveyed from the windward side. This phenomenon subsequently induces a widespread upward motion of the airflows within the recirculation zone. However, the temperature rise on the leeward side is not as significant as on the roof surface. The temperature near the leading edge of the roof and within the recirculation region is higher, indicating a more pronounced influence of buoyancy flow.

In light of the combined influence of different heating temperatures and incoming wind speeds, the temperature distribution at pedestrian height is depicted in Fig.7 when all walls are heated. Upon heating all walls, a notable synergistic relationship between temperature and incoming wind speed becomes evident, resulting in a spatial overlap between high-temperature areas and regions characterized by low wind speeds. When the wall heating temperature is relatively high, especially at the four corner positions of the isolated building, local high-temperature areas are formed due to the lower wind speed. At an incoming wind speed of 0.5 m/s, the thermal airflow primarily converges at the four corner positions of the isolated building and within the wake region. Nevertheless, with the escalation of incoming wind speeds to 1 m/s and 2 m/s, and coupled with an increase in wall heating temperature, the thermal airflow extends downstream of the isolated building. Of particular note, under the condition of *Ri*=1.00, the thermal airflow at the pedestrian height level has the widest range of effects, while the high-temperature areas around the isolated building show the greatest range.

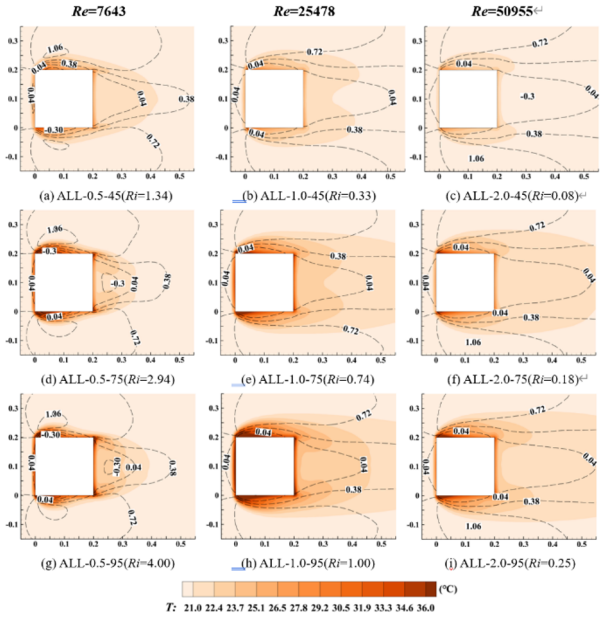

Fig. 7. Time-averaged temperature over the horizontal plane at z/H_b=0.15 (the long-dashed lines represent the contour of the normalized time-averaged U_x; the dimensions are in [m]).

5 Discussion

The investigation of flow field around a building exhibiting varying thermal effects is conducted in wind tunnels by heating up building surfaces. The relative magnitudes of the *Ri* are controlled by setting appropriate wall heating temperatures and choosing representative speeds of approaching flow. By conducting case studies in a similar format, it is possible to unveil general patterns and fundamental phenomena. While this method does not necessarily replicate the realistic temperature distribution in outdoor environments, it allows for better control of the building surface temperature and ensures repeatability [46]. Furthermore, wind tunnel test data with thermal effects can be used to validate numerical simulation results. Once validated, these numerical models can be employed to replicate challenging cases that are difficult to achieve in wind tunnel tests. The LES method is capable of accurately simulating the wind and thermal conditions around the isolated building. It allows for capturing the turbulent nature of the airflow around the isolated building, providing a holistic understanding of the phenomenon.

Buoyant flow can alter the flow patterns around the isolated building. While moderate heating of the building surfaces has a minimal impact on the surrounding flow field, vortex circulation within the recirculation region does accelerate with increased heating temperatures. Comparing the lengths of the recirculation region under identical incoming wind speed and heating temperature reveals that all-wall heating results in the most significant reduction, potentially halving the length compared to the non-heated condition. This is followed by heating the windward wall, with the leeward wall heating producing the least reduction in the recirculation region.

When all walls are heated, increasing the temperature initially reduces the length of the recirculation region (except for ALL-0.5-75 and ALL-0.5-95), but it then enlarges subsequently, as summarized in Fig.8. Heating the leeward wall diminishes the length of the reattachment region on the roof, while heating either the windward wall or all walls lead to an increase in the length of the reattachment region. From Fig. 8(a)-(c), in any case of wall heating, a decrease in *Re* significantly reduces the length of the recirculation region, especially when all walls are heated. This observation aligns with the findings of Ruck [26] in their analysis of the flow field around a heated building model in a wind tunnel. At *Re*=50955, heating the windward, leeward, or all walls to different temperatures has minimal influence on the lengths of both recirculation and reattachment regions. As mentioned earlier, under high *Re* conditions, forced convection dominates, and thermal effects have minimal impact. In contrast to previous studies, there was no observed temperature accumulation in the low-speed core of the wake vortex when only the leeward wall was heated. With regard to vortex core locations, both the top vortex and the wake vortex tend to move upwards and downstream as buoyancy effect becomes more pronounced.

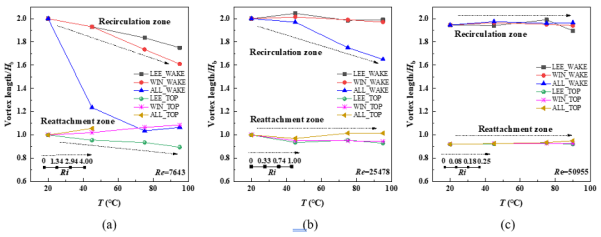

Fig. 8. Comparison of the lengths of the recirculation and reattachment regions when heating leeward, windward and all walls at (a) *Re*=7643 (In the ALL-TOP condition, when *Ri* = 2.94 and 4.00, the flow structures on the roof are destroyed by buoyant flows and the reattachment region disappears), (b) *Re*=25478, (c) *Re*=50955.

For all studied conditions, heating the building walls has a minimal impact on the flow upstream of the building, and the temperature rapidly decays in the vicinity of the heated wall. Under high *Re* (*Re*=50955), the flow characteristics of different cases are similar to the case where no heating is applied.

In Fig. 9, we present a visualization that depicts the distribution of vorticity magnitude across various heating conditions, which effectively identifies and locates vortices. In the absence of heating, the strength of the horseshoe vortex in front of the building is prominent. However, during heating conditions, this vortex weakens, with the phenomenon being most pronounced when all walls are heated. When heating either the leeward wall or all walls, there is a significant reduction in vortex strength near the ground on the leeward side. Simultaneously, an increase in vortex intensity is observed within the roof shear layer. This phenomenon can be attributed to the enhanced rotational motion of the airflow influenced by buoyancy.

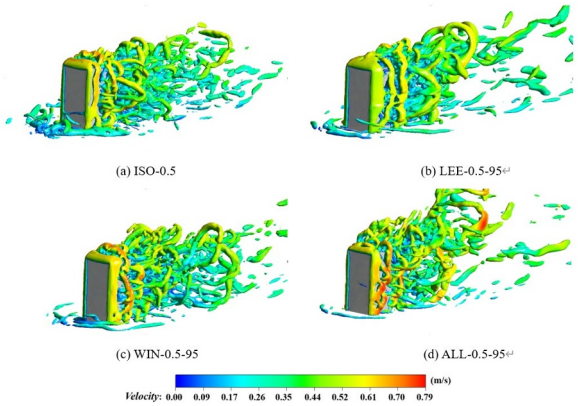

Fig. 9. Vorticity iso-surface distribution from *Q*-Criterion: (a) ISO-0.5, (b) LEE-0.5-95, (c) WIN-0.5-95, and (d) ALL-0.5-95, with velocity values colored on the iso-surfaces (the iso-surface corresponds to *Q*=11.8, *Re*=7643, *Ri*=4.00).

6 Conclusion

This study investigates the impact of buoyancy flow on the flow field around an isolated cubic building with heated surfaces using LES. The simulation results are validated through wind tunnel tests. The study focuses on low wind speed conditions ranging from 0.5 to 2 m/s. The windward, leeward, and all walls of the building are heated, resulting in an increase in surface temperature from 20 °C to 95 °C. The corresponding *Ri* ranges from 0 to 4.00. The combination of numerical simulations and wind tunnel tests in a case-study format aims to uncover general trends and fundamental phenomena. This research approach enables better control and reproducibility of the building surface temperature. The numerical simulation conditions and experimental methods employed in this study serve as valuable guidance for future research endeavors.

Based on the analysis above, it can be concluded that forced convection plays a dominant role in the low *Re*, while buoyancy flow has a minimal effect. The maximum value of *Ri*, which corresponds to the flow characteristics primarily governed by forced convection, is referred to as the critical *Ri*. This critical value is derived from a limited number of cases in this study, and future research can explore additional cases to determine critical *Ri*. It is conceivable that different regions around the building may have distinct critical *Ri* values under varying heating conditions.

When the leeward wall is heated, most of the heat is carried away vertically by the thermal plume. Upon heating the windward wall, specifically under the *Ri*=4.00 condition, results in the majority of the heat being entrained into the near wake through the recirculation region, causing a rise in temperature on the leeward side. When all the walls are heated at *Ri*=1.34, the wake vortex is perturbed due to the buoyancy flow, but the top vortex remains unaffected. At *Ri* = 2.94 and 4.00, both the wake and top vortex structures become disrupted. Additionally, when the windward wall and all walls are heated, particularly under the *Ri* = 4.00 condition, the thermal plume near the windward wall is strong enough to counteract the downward inertial force, resulting in visible upward motion of the thermal plume.

In conclusion, the analysis conducted in this study on the influence of thermal effects on the flow field characteristics offers potential integration with research on architectural planning and pollutant dispersion. For instance, while high k promotes the mixing of air and heat transfer, it simultaneously results in an elevated rate of pollutant diffusion within buildings. An optimally structured flow field facilitates the intake of fresh air and the expulsion of pollutants, thereby improving urban air quality and minimizing pollutant buildup. This research sheds light on the dynamics of airflow and temperature distribution in outdoor microenvironments. It is crucial to account for the interplay between incoming wind speed and heating temperature. Emphasis is especially placed on the building's corners and proximate wall areas, as they may be pivotal in the aggregation and distribution of thermal airflows at pedestrian level. Indeed, this paper explores an idealized scenario. In practical situations, nearby structures are expected to exert a discernible influence on the airflow around the isolated building. For instance, adjacent buildings may cause obstructions to the isolated building. Future investigation endeavors will delve deeper into this particular aspect.

Acknowledgement

This work was supported by the National Natural Science Foundation of China under the project number of 52078353, the Research Scheme of Research Grant Council of Hong Kong SAR, China (NO. T22-504/21R), the National Key Research and Development Program of China (NO. 2023YFC3805304-2), and International Cooperation project of Science and Technology Commission of Shanghai Municipality (NO. 22200711400).

References

1. K. Zhang, C. Cao, H. Chu, L. Zhao, J. Zhao, X. Lee, Nature. **617**, 738-742 (2023)
2. S. Murakami S, A. Mochida, Y. Hayashi, S. Sakamoto. J Wind Engi Ind Aerod. **44**, 2841-2852 (1992).
3. T. Okaze, H. Kikumoto, H. Ono, M. Imano, N. Ikegaya, T. Hasama, Build Environ. **202** 108021 (2021).
4. Y. Lin Y, J. Hang, H. Yang, L. Chen, G. Chen, H. Ling, M. Sandberg, L. Claesson, CKC. Lam, Build Environ. **201**, 107965 (2021).
5. C. Tsalicoglou, J. Allegrini, J. Carmeliet, J Wind Eng Ind Aerod. **204**, 104248 (2020).
6. J. Allegrini, V. Dorer, J. Carmeliet, Build Environ **59**, 315-326 (2013).
7. M. Antonopoulosdomis, J Fluid Mech, **104**, 55-79 (1981)
8. F. Baetke, H. Werner, H. Wengle, J Wind Eng Ind Aerod, **35**, 129-147 (1990).
9. Y. Zhao, R. Li, L. Feng, Y. Wu, J. Niu, N. Gao, Renew Sust Energ Rev, **167**, 112717 (2022)
10. B. Ruck, J Wind Eng Ind Aerod, **50,** 139-152 (1993)